Available online at www.sciencedirect.com
SCIENCE DIRECT®
International Journal of Thermal Sciences 45 (2006) 553–566
International Journal of Thermal Sciences
www.elsevier.com/locate/ijts

Radiation—natural convection heat transfer in an inclined rectangular enclosure

H. Bouali [a], A. Mezrhab [a,*], H. Amaoui [a], M. Bouzidi [b]

[a] *Faculté des Sciences, Département de Physique, Laboratoire de Mécanique & Energétique, Université Mohammed 1er, 60000 Oujda, Morocco*
[b] *Université Clermont Ferrand 2, IUT, av. A. Briand, 03107 Montluçon cedex, France*

Received 22 February 2005; received in revised form 18 May 2005; accepted 3 October 2005

Available online 14 November 2005

Abstract

In this paper, the effects of surface radiation and inclination angle on heat transfer and flow structures in an inclined rectangular enclosure have been studied numerically. The governing differential equations were solved by a finite volume method. The SIMPLER algorithm was used for the velocity-pressure coupling, and the view factors were determined by a boundary element approximation and a Monte Carlo method. The vertical walls of the enclosure are heated with uniform different temperatures and the others are adiabatic. The enclosure is inclined and contains a centred inner body, for which the effects of thermal conductivity on heat transfer and air flow were analysed. It was found that the increase of the inclination angle reduces considerably the total heat transfer in the cavity, the effect of the inner body thermal conductivity k_{ib} depends on the inclination angle ϕ, and the inner body reduces the heat transfer in the cavity especially in the presence of radiation exchange.

Keywords: Natural convection; Surface radiation; Inclined enclosure; Inner body

1. Introduction

Natural convection in a partitioned cavity has been extensively studied using numerical simulations and experiments because of its interest and importance in industrial applications [1–7]. Some applications are solar collectors, fire research, electronic cooling, aeronautics, chemical apparatus, building construction, nuclear engineering, etc.

Natural convection in an inclined rectangular enclosure has also attracted a lot of attention. In their investigation, Ramos et al. [8] analysed the steady-state flow in a square two-dimensional thermosyphon. They studied the effect of the temperature differences and inclination angles on the flow patterns. They demonstrated the existence of multiple solutions, and found recirculating flow under particular conditions. Kimura et al. [9] investigated both experimentally and numerically the natural convection heat transfer in a rectangular inclined cavity with a centred conducting body. They have varied parametrically the thermal conductivity ratio R_k, and found that the inner body with a large thermal conductivity enhances the heat transfer in the enclosure at large inclination angles, while it suppresses the heat transfer for small inclination angles of the enclosure.

The first numerical study of the coupled heat transfer problem involving both convection and radiation in a rectangular cavity seems to be that of Larson and Viskanta [10]. They found that radiation heats up the cavity surface and the gas body very quickly and thus considerably modifies the flow pattern and the corresponding convection process. Later, Lauriat [11,12] used the $P-1$ differential approximation to represent radiative heat transfer in narrow vertical cavities. Yücel et al. [13] used the discrete ordinates method to study combined natural convection and radiation heat transfer from a scattering medium in a square enclosure. Since, the interaction between natural convection and radiation with or without participating media in the case of an undivided cavity has been studied by many researchers [14–18]. These studies are accomplished by different methods, but only restricted to 2D geometries. Lately, Colomer et al. [19], have analysed, in a three-dimensional, differentially heated cavity, the combined natural convection-radiation by us-

* Corresponding author. Tel.: +212 56 50 06 01/02; fax: +212 56 50 06 03.
E-mail address: mezrhab@sciences.univ-oujda.ac.ma (A. Mezrhab).

1290-0729/$ – see front matter
doi:10.1016/j.ijthermalsci.2005.10.001

Nomenclature

A	cavity aspect ratio, $A = L/b$	
A^*	body aspect ratio, L_i/b_i	
A_i	radiative surface number i	
b	enclosure width	m
b_i	width of the inner body	m
F_{i-j}	view factor between A_i and A_j	
g	gravity acceleration	$\mathrm{m{\cdot}s^{-2}}$
L	enclosure length	m
L_i	length of the inner body	m
k	thermal conductivity	$\mathrm{W{\cdot}m^{-1}{\cdot}K^{-1}}$
N	total number of radiative surfaces	
Nr	radiation number, $\sigma T_h^4/(k_f \Delta T/b)$	
Nuw	average Nusselt number	
$Nu(Y)$	local Nusselt number along the Y-axis	
p	pressure	Pa
P	dimensionless pressure, $(p + \rho_o g y)L^2/\rho_o \alpha$	
Pr	Prandtl number, ν/α	
q_w	heat flux at the isothermal walls	$\mathrm{W{\cdot}m^{-2}}$
q_r	net radiative flux density	$\mathrm{W{\cdot}m^{-2}}$
Q_r	dimensionless net radiative flux density, $q_r/\sigma T_h^4$	
Ra	Rayleigh number, $g\beta(T_h - T_c)b^3/\nu\alpha$	
R_i	dimensionless radiosity of surface A_i	
R_k	thermal conductivity ratio, k_{ib}/k_f	
T	temperature	K
T_o	average temperature, $(T_h + T_c)/2$	K
u, v	velocity components	$\mathrm{m{\cdot}s^{-1}}$
U, V	dimensionless velocity components, $(U = ub/\alpha,\ V = vb/\alpha)$	
x, y	Cartesian coordinates	m
X, Y	dimensionless Cartesian coordinates, $(X = x/b,\ Y = y/b)$	

Greek symbols

α	thermal diffusivity of the fluid	$\mathrm{m^2{\cdot}s^{-1}}$
β	volumetric expansion coefficient	$\mathrm{K^{-1}}$
ϕ	inclination angle	degrees
ΔT	maximal difference temperature, $(T_h - T_c)$	K
$\Delta\theta$	step of isotherms	
$\Delta\psi$	step of streamlines	
ε_i	emissivity of surface A_i	
ν	kinematic viscosity of the fluid	$\mathrm{m^2{\cdot}s^{-1}}$
ρ_o	density of the fluid at T_o	$\mathrm{kg{\cdot}m^{-3}}$
Θ	dimensionless temperature, T/T_h	
θ	dimensionless temperature, $(T - T_c)/\Delta T$	
σ	Stefan–Boltzmann constant	$\mathrm{W{\cdot}K^{-4}{\cdot}m^{-2}}$

Subscripts

c	cold
f	fluid
h	hot
ib	inner body
nb	cavity without an inner body
s	solid
w	walls of the cavity
wb	cavity with an inner body

ing the discrete ordinates method (DOM) to solve the radiative transfer equation. Both transparent and participating media are discussed, and the effects of Planck and Rayleigh numbers, as well as the optical thickness, are studied.

In the case of partitioned cavities, there are few studies on the coupled heat transfer problem involving both convection and radiation. However, it is well known that when natural convection in air is involved, the heat transfer by natural convection and radiation are usually of the same order of magnitude. Early investigations of the combined natural convection-surface radiation in a partitioned cavity have been carried out by Chang et al. [20] who treated the radiation natural convection interaction phenomena in square enclosures with equal vertical finite-thickness partitions located at the centres of the ceiling and floor. Both surface and gas radiation effects were examined. It is shown that the predominant mechanism by which the radiation process enhances the overall heat transfer rates is the surface radiation. Nakamura and Asako [21] conducted a numerical and experimental study on the effect of a partition, which has zero thickness and located vertically at the midpoint of the differentially heated cavity. It was found that the emissivities of the top and bottom walls only slightly affect the heat transfer by convection in both cases of conductive and insulated top and bottom walls. On the other hand, the emissivities of the cold and hot walls and of the partition were shown to considerably modify the convective heat transfer. Mezrhab and Bchir [22] studied the effects of adding a thick partition located vertically close to the hot wall of a differentially heated square cavity, forming a narrow vertical channel in which the flow is controlled by vents at the bottom and the top of the partition. It is shown that radiation has a significant influence on the flow and heat transfer in the channel. Recently, Han et al. [23] numerically studied natural convection of a radiating fluid in a rectangular enclosure, with two incomplete adiabatic thin partitions (one on the top and the other at the bottom) under a large temperature difference. They have used the finite-volume method (FVM) to solve the radiative transport equation, and have found that the radiation alters significantly the flow patterns and the thermal distributions. In addition, the surface radiation was dominant over the gas radiation and the results were affected by the baffle configuration. Finally, Mezrhab et al. [24,25] presented a numerical study, based on a finite volume method and a boundary element approximation, of the radiation-natural convection interactions in a differentially heated square enclosure, within which a centred, squared, heat-conducting body generates heat. They found that the streamlines and isotherms structures in the enclosure are strongly affected by the thermal radiation heat transfer. Moreover, this one increases considerably the total

heat transfer in the enclosure, and allows a good cooling of the body that generates heat.

The main purpose of this paper is the analysis of radiation-natural convection interactions in a differentially heated rectangular cavity containing a centred conducting body. In comparison to the previous studies achieved on the partitioned cavity, our contribution lies in the fact that the enclosure is of an aspect ratio equal to 2 and it is inclined by an angle ϕ with respect to the horizontal. In addition a complete parametric study is made for different inclination angles, conductivities of the body, Rayleigh numbers, and emissivities of walls when taking into account the radiation heat transfer.

2. Mathematical formulation and computational procedure

The studied geometry is shown in Fig. 1. The flow is assumed to be incompressible, laminar and two-dimensional in a rectangular enclosure with an aspect ratio $A = 2$, the horizontal end walls are perfectly insulated while the two vertical walls are maintained at two different temperatures T_h and T_c respectively. The working fluid is air with physical properties, except the density, constant at the average temperature T_o. Indeed, it is the buoyancy force generated by the density gradient that is responsible of the fluid motion inside the enclosure. The radiative surfaces of the enclosure and the body are assumed diffuse-gray.

The governing equations are non-dimensionalized using the following definitions of the dimensionless variables:

$$X = x/b, \quad Y = y/b$$

$$U = ub/\alpha, \quad V = vb/\alpha$$

$$\theta = (T - T_c)/(T_h - T_c), \quad P = (p + \rho_o g y)b^2/\rho_o \alpha^2$$

Then the dimensionless governing equations for the present system can be expressed by the following steady, two-dimensional equations:

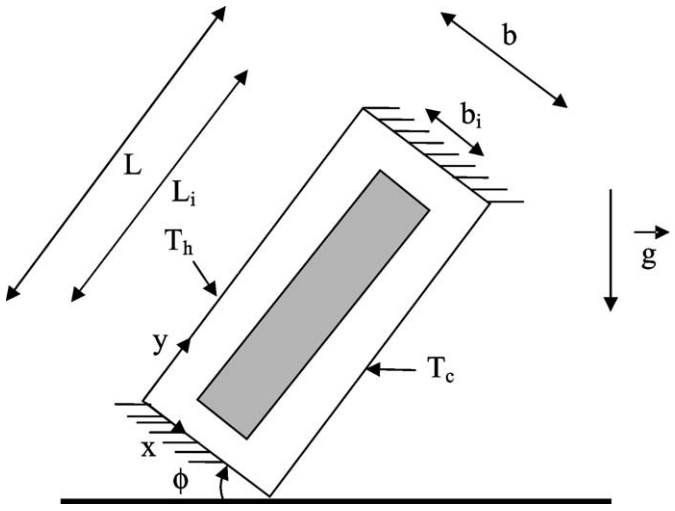

Fig. 1. Geometry of the inclined cavity.

Continuity:

$$\frac{\partial U}{\partial X} + \frac{\partial V}{\partial Y} = 0 \tag{1}$$

X momentum:

$$U\frac{\partial U}{\partial X} + V\frac{\partial U}{\partial Y} = -\frac{\partial P}{\partial X} + \lambda Pr\left(\frac{\partial^2 U}{\partial X^2} + \frac{\partial^2 U}{\partial Y^2}\right) - Ra\,Pr\,\theta \sin\phi \tag{2}$$

Y momentum:

$$U\frac{\partial V}{\partial X} + V\frac{\partial V}{\partial Y} = -\frac{\partial P}{\partial Y} + \lambda Pr\left(\frac{\partial^2 V}{\partial X^2} + \frac{\partial^2 V}{\partial Y^2}\right) + Ra\,Pr\,\theta \cos\phi \tag{3}$$

Energy:

$$U\frac{\partial \theta}{\partial X} + V\frac{\partial \theta}{\partial Y} = R_k\left(\frac{\partial^2 \theta}{\partial X^2} + \frac{\partial^2 \theta}{\partial Y^2}\right) \tag{4}$$

λ and R_k are equal to 1 in the fluid region and $\lambda = \infty$, $R_k = k_{ib}/k_f$ in the inner body.

Hot and cold walls are maintained at dimensionless temperature of 1 and 0, respectively. For the velocity field, the boundary conditions are the no-slip type. The inclination angle ϕ is taken positive in the clockwise direction.

The numerical solution of the governing differential equations for the velocity, pressure and temperature fields is obtained by using a finite volume technique. The latter utilizes a second-order central difference scheme (CDS) for the convective terms in order to reduce numerical diffusion errors. In the range of Rayleigh numbers investigated, the CDS solution did not exhibit spurious oscillations and the convergence was achieved by using small under-relaxation factors on U, V and θ. The simpler algorithm (semi-implicit method for pressure linked equations revised) described in detail by Patankar [26] is employed to solve the coupling between pressure and velocity. The governing equations were cast in transient form and a fully implicit transient differencing scheme was employed as an iterative procedure to reach a steady state. The presence of an inner body was accounted for by the strategy in which a region of high viscosity characterizes it.

The discretized equations obtained are solved iteratively by an algorithm based on a preconditioned conjugate gradient method. The solution is considered to be fully convergent when the steady state is achieved, i.e. in this study when the maximum absolute value of $(\varphi^{(n+1)} - \varphi^{(n)})$ is smaller than 10^{-6} where φ is a dependent variable that represent U, V or θ, and n is the iteration number (i.e. false time step). For the pressure correction equation, which is a discretized Poisson equation, the iterative process was stopped when the maximum residual of mass (amount by which the continuity equation was not satisfied) was less than 10^{-8}.

For the radiative heat transfer problem, the working fluid (air) is considered to be perfectly transparent. Thus, the air does not participate in the radiative heat transfer, and only the solid surfaces contribute to the radiation exchange. These surfaces

are assumed to be diffuse-gray. In this case, indeed, one knows that the radiative transfers appear in the heat balance of the system only on the level of the boundary conditions. Thus, after having established the boundary conditions, which describe the radiative exchanges between surfaces, the problem is to evaluate the radiative heat flux, which comes in the expression of the assessment of energy at the border of the solid node. The enclosure walls and the inner body boundaries are divided into finite number of zones on which the four basic assumptions of the simplified zone analysis were assumed valid. The number of zones retained was determined by the mesh used to solve the differential equations. Indeed, the grid was constructed such that the boundaries of physical domain coincided with the velocity grid lines. The points for pressure and temperature were placed at the center of the scalar volumes. At the fluid–solid interfaces, the control volume faces were also arranged so that a control volume face coincided with an interface solid–fluid. Therefore, the zoning was not uniform and the area of each zone varied according to the stretching function and number of grid points used. This grid distribution was chosen to ensure the interface energy balance. To avoid a checkerboard pressure and velocity field a staggered grid for velocity is used.

Determination of the net radiative flux density requires the knowledge of the surface temperature of each node. The equation of the thermal balance of each surface provides us with these temperatures. Thus, one assumes that the solid surfaces are in thermal equilibrium under the combined action of the conductive, convective and radiative contributions, which give:

$$k_s \frac{\partial T_s}{\partial z} = k_f \frac{\partial T}{\partial z} - q_r \tag{5}$$

where z denotes the normal direction to the interface under consideration and q_r the net radiative flux density along this interface. In dimensionless form and with using the dimensionless variable ($Z = z/b$), Eq. (5) can be written:

$$R_k \frac{\partial \theta_s}{\partial Z} = \frac{\partial \theta}{\partial Z} - Nr Q_r \tag{6}$$

For the insulated walls, $Z \equiv Y$ and Eq. (6) becomes:

$$\frac{\partial \theta}{\partial Y} - Nr\, Q_r = 0 \tag{7}$$

In order to discretize Eqs. (6) and (7), the radiative surfaces of the solid forming the enclosure and the inner body are divided into a number of surfaces A_i, $i = 1, N$. N is the number of total radiative surfaces forming the cavity and the inner body boundaries, which are equal to the total control volume interfaces solid–air. The surface temperatures were updated from the solution of the energy equation by under-relaxing the boundary evaluation of temperature.

Therefore, the dimensionless net radiative flux density along a diffuse-gray and opaque surface "A_i" is expressed as:

$$Q_{r,i} = R_i - \sum_{j=1}^{N} R_j F_{i-j} \tag{8}$$

For N radiative surfaces, this results in $N(N-1)/2$ view factors F_{i-j} to be calculated and in a linear system of N equations for the radiosities. The view factors were determined by using a boundary element approximation to fit the surfaces and a Monte Carlo method for the numerical integrations [27].

R_i is the dimensionless radiosity of surface A_i, obtained by resolving the following system:

$$\sum_{j=1}^{N} \left(\delta_{ij} - (1-\varepsilon_i) F_{i-j}\right) R_j = \varepsilon_i \Theta_i^4 \tag{9}$$

with δ_{ij} the Kronecker symbol.

The average Nusselt number along the hot wall is defined as:

$$Nuw = \frac{1}{A} \int_0^A \left(-\left.\frac{\partial \theta}{\partial X}\right|_{0,Y} + N_r Q_r(0, Y) \right) \mathrm{d}Y \tag{10}$$

3. Grid size sensitivity test

Geometry studied in this paper is an obstructed cavity; therefore several grid size sensitivity tests were conducted in this geometry to determine the adequacy of the mesh scheme and to ensure that the solutions are grid independent. This is obtained when numerical results of the average Nusselt number *Nuw* become grid size independent, although we continue the refinement of the mesh grid.

As can be seen in Table 1, six non-uniform grid sizes were considered. Since the enclosure contains an inner body, its computational domain is divided into three parts in the Y direction and three parts in the X direction. In the Y direction, the first part represents the region that is downstream of the inner body, the second part coincides with the inner body height, and the third part is the region upstream of the inner body. In the X direction, the first part is located between the hot wall and the left boundary of the inner body, the middle part coincides with the inner body width, and the last part is the region separating the right boundary of the inner body and the cold wall. The number of control volumes used in each part is presented in parentheses (for the X-direction, the data in parentheses are ordered from the left to the right of the enclosure and for the Y-direction, they are ordered from the downstream to the upstream of the enclosure). For example, for the first grid given in Table 1, 6×14 control volumes are used for the inner body.

As is shown in Table 1, a 42×48 control volumes can be chosen to optimize the relation between the accuracy required

Table 1
Grid sensitivity test (pure natural convection case: $\varepsilon = 0$), $Ra = 5 \times 10^4$ and $Pr = 10$

X-direction	Y-direction	*Nuw*
22(8, 6, 8)	26(6, 14, 6)	3.263
28(10, 8, 10)	32(8, 16, 8)	3.294
34(12, 10, 12)	38(10, 18, 10)	3.311
42(18, 6, 18)	48(8, 32, 8)	3.319
52(18, 16, 18)	56(16, 24, 16)	3.334
58(20, 18, 20)	60(18, 26, 16)	3.335

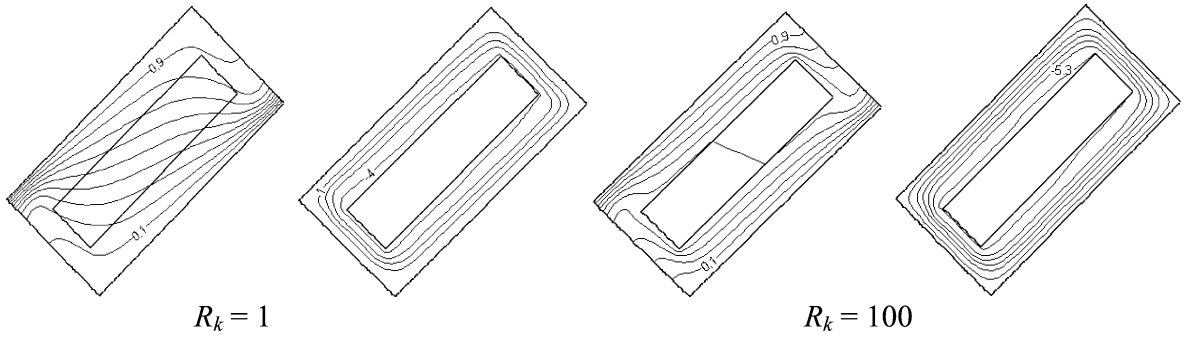

(a) $Ra = 5\times10^4$ and $\phi = 45°$

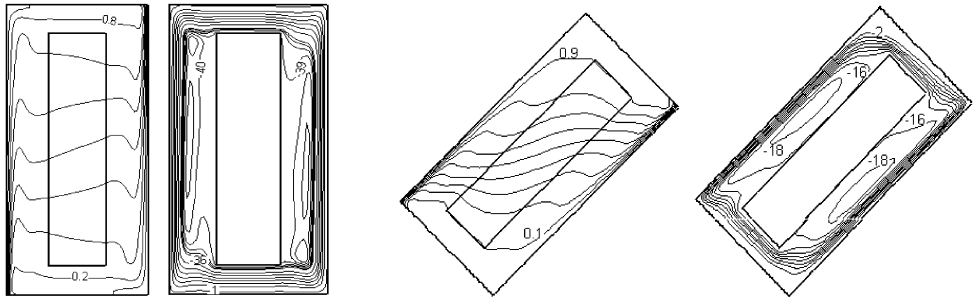

(b) $Ra = 5\times10^6$ and $R_k = 1$

Fig. 2. Isotherms and streamlines for $Pr = 10$.

and the computing time. Indeed, the maximum difference between the values of *Nuw* obtained for the 42×48 grid and the finest 58×60 grid was less than 0.5%.

The mathematical model developed in the last section was used to investigate the mutual interaction radiation-natural convection in an inclined enclosure.

4. Code validation

The code was extensively exercised on benchmark problems to check its validity. We recall here some results obtained by our code in comparison with those reported in Ref. [9] for $\phi = 0°$, 45° and two values of $R_k = 1$ and 100 (see Figs. 3, 4, 5 and 6 in Ref. [9]).

Firstly, the code validation was achieved for isotherms and streamlines patterns, in inclined and vertical cavities. As in Ref. [9] we consider two different Rayleigh numbers ($Ra = 5 \times 10^4$ and $Ra = 5 \times 10^6$). Isotherms and streamlines presented in Fig. 2 can be favourably graphically compared with those presented in Ref. [9] by studying the same problem and by taking the same values for the parameters that are used. Secondly, we have compared results of the inclination angle effect on the average Nusselt number as a function of the thermal conductivity ratio R_k for $Ra = 5 \times 10^4$, obtained by our code (see Fig. 3) with those presented in Fig. 10 of Ref. [9]. There also, we obtained an excellent agreement.

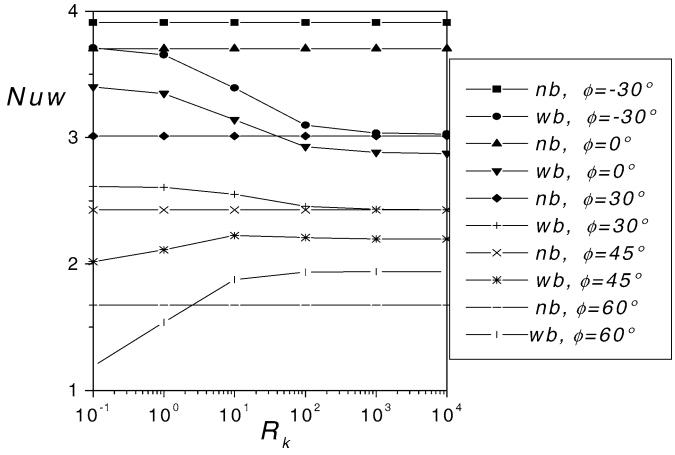

Fig. 3. Relation between R_k and average Nusselt number *Nuw* for $Pr = 10$ and $Ra = 5 \times 10^4$.

When the radiation exchange is taken into account, the presented numerical study was checked for accuracy against the numerical results earlier published and reported by different authors, and the agreement between the present and the previous results was very good as indicated in Ref. [25]. In this paper, we limit ourselves to compare our results with those obtained by Chang et al. [20]. The enclosure geometry treated in Ref. [20] is shown in Fig. 4. The enclosure is a square differentially heated with identical vertical finite thickness partitions located at the centers of the ceiling and floor. The vertical walls are main-

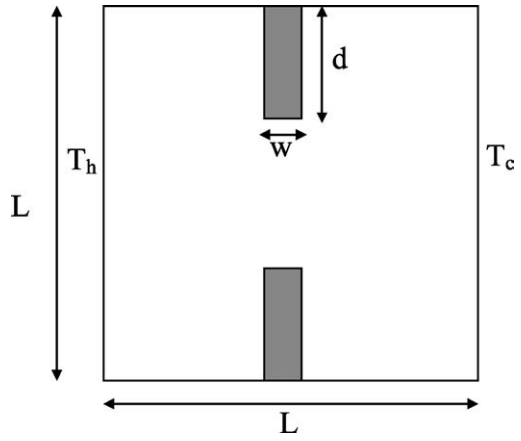

Fig. 4. Geometry considered for the code validation.

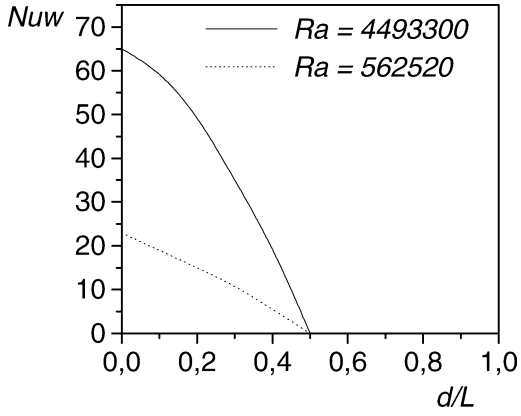

Fig. 5. Average Nusselt number *Nuw* versus d/L for $Ra = 4493300$ and 562520.

tained isothermal with $T_h > T_c$ while the horizontal walls and the partitions are assumed to be adiabatic. All radiative surfaces are considered as black. The width w of the partitions is equal to $L/10$ (L is the height of the enclosure). Temperatures of the cold and hot walls are respectively $T_c = 277.8$ K and $T_h = 833.4$ K. We present in Fig. 5, the average Nusselt number *Nuw* for various dimensionless partition heights (d/L) and for two Rayleigh numbers $Ra = 4493300$ and 562520. This figure can be favourably graphically compared with curves corresponding to the case of air-surface radiation displayed respectively in Fig. 7 for $Ra = 4493300$ and in Fig. 8 for $Ra = 562520$ in Ref. [20].

Based on the above studies, it was concluded that the code could be reliably applied to the considered problem.

5. Results and discussion

In this investigation, both cases of pure natural convection and natural convection coupled with surface radiation are presented. Each case required the specification of four dimensionless parameters ($\varepsilon, \phi, \Delta T, R_k$); the others parameters such as Prandtl number, average temperature, cavity width, inner body height, inner body width, and cavity aspect ratio are respectively held fixed to $Pr = 0.70$, $T_o = 300$ K, $b = 0.03$ m, $L_i = 0.8L$, $b_i = 0.4b$, and $A = 2$.

5.1. Results without radiation ($\varepsilon = 0$)

In this case there is no heat transfer by radiation ($\varepsilon = 0$). Therefore, we treat the effect of the three parameters (ϕ, ΔT, R_k) on the pure natural convection heat transfer in inclined cavity. For this reason we fix two parameters to study the effect of the remaining one.

5.1.1. Effect of ϕ

The effect of the inclination angle ϕ is investigated with the following parameters: maximal difference temperature, $\Delta T = 30$ K and thermal conductivity ratio, $R_k = 1$. The Rayleigh number deduced from the value of $\Delta T = 30$ K is $Ra = 7.5 \times 10^4$. Fig. 6 shows the effect of ϕ (ϕ chosen here are 60, 0 and -60 degrees) on the computed isotherms and streamlines structures. For a purpose of comparison, the case of an empty cavity is also presented.

In each case, the flow circulates in the clockwise direction owing to the position of hot and cold walls. Indeed, the flow rises along the hot wall and descends along the cold one. The angle of tilt ϕ has a dramatic influence on the flow housed by the enclosure.

At $\phi = 60°$, the isotherms in the inner body are nearly perpendicular to the gravitation, which yields the heat to be transferred in parallel with the gravitation through the inner body. These isotherm structures are quite similar to those obtained in the case of an empty cavity. In fact, at $\phi = 60°$ the convection currents are weak and conduction is the predominant mode of heat transfer, so since the inner body has the same thermal conductivity as the air ($R_k = 1$), its effect on the isotherms is almost negligible. As for the streamlines, the presence of the inner body has a slight effect on the flow structures. This is because the inner body is located at the central region of the cavity which is nearly stagnant for $\phi = 60°$.

For both cases (*wb* and *nb*), Fig. 6 suggests that as ϕ decreases from 60° to 0° or $-60°$, the heat transfer mechanism switches from a conduction mode to single-cell convection at $\phi = 0°$ and to a mode nearer to the Bénard convection at $\phi = -60°$. The inner body modifies much the temperature fields. Indeed, at $\phi = 0°$, the isotherms which are nearly horizontal in the empty cavity become inclined in a partitioned cavity; whereas at $\phi = -60°$, they change from inclined in the empty cavity to horizontal in the partitioned one. At $\phi = 0°$, as well as in the case $\phi = 60°$, the inner body has a slight effect on the streamlines because the region that it occupies is nearly stagnant even in the empty cavity. However, at $\phi = -60°$, the stronger convective motion developed in the central region of the empty cavity is prevented by the inner body in the case of the partitioned cavity.

Now, if we focus attention upon the effect of the inclination angle ϕ on the conduction heat transfer in the inner body, the isotherm structures in it reveal that at high ϕ ($\phi = 60°$) the heat is transferred from the left surface of the inner body (facing the cavity hot wall) to the right one (facing the cavity cold wall), while at low values of ϕ the heat is transferred through the inner body from its top to its bottom boundary. This is due to the closeness of the temperatures of the inner body boundaries

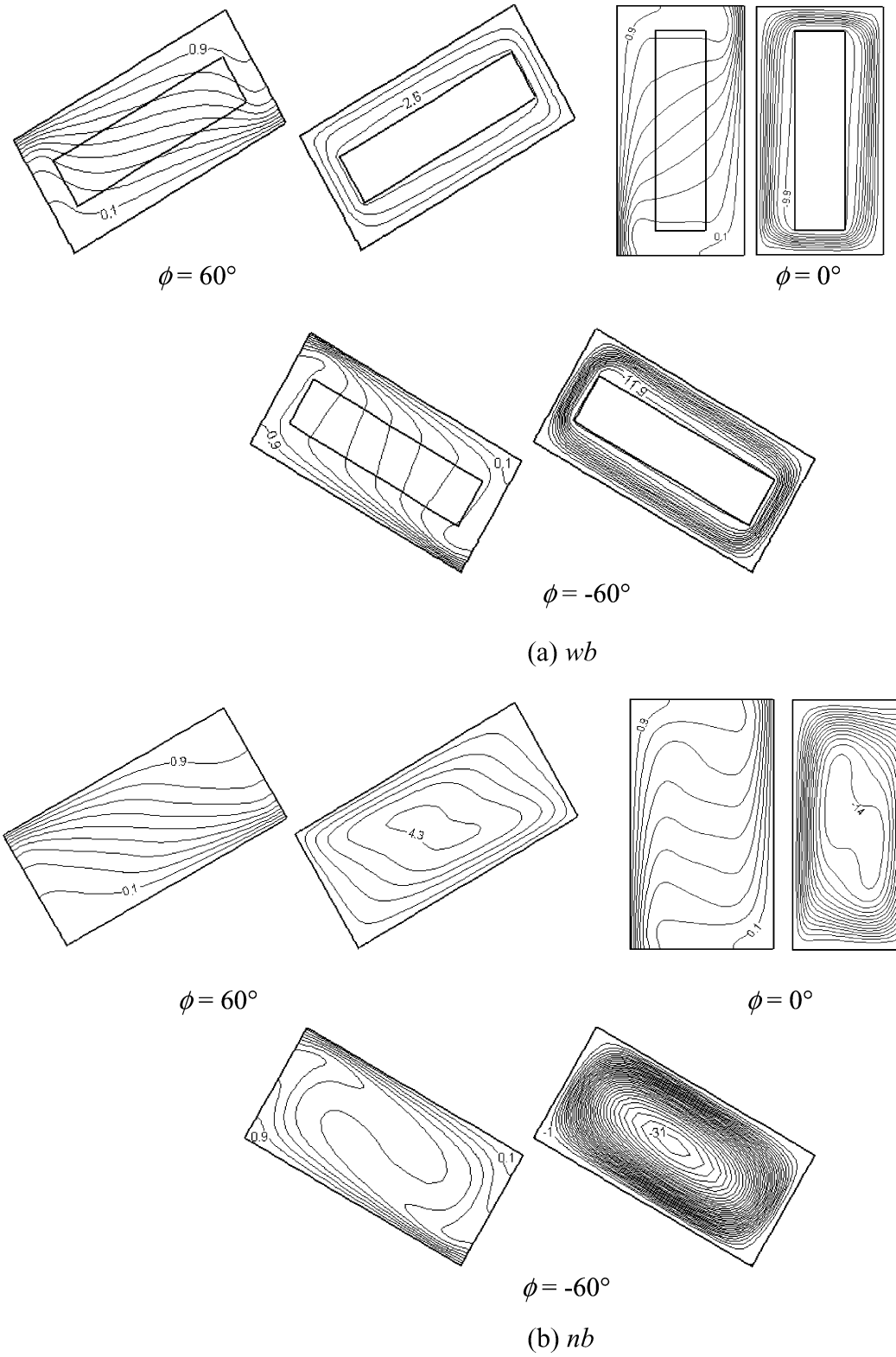

Fig. 6. Isotherms and streamlines for $Ra = 7.5 \times 10^4$, $R_k = 1$, $\Delta\theta = 0.1$ and $\Delta\psi = 1$.

facing hot and cold cavity walls when ϕ is weak as shown in Fig. 7.

The variation of the local Nusselt number on the hot wall ϕ ($-60°$, $0°$ and $60°$), is shown in Fig. 8(a) for a partitioned cavity and in Fig. 8(b) for an empty one. It can be seen that the decrease of ϕ from $60°$ to $0°$ or $-60°$ enhances largely $Nu_{wb}(Y)$. This enhancement is more important near the bottom hot wall. Indeed, at low values of ϕ, the circulation induced by the buoyancy force is important as shown in Fig. 6. This means an increase of the mass flow rate through the opening bounded

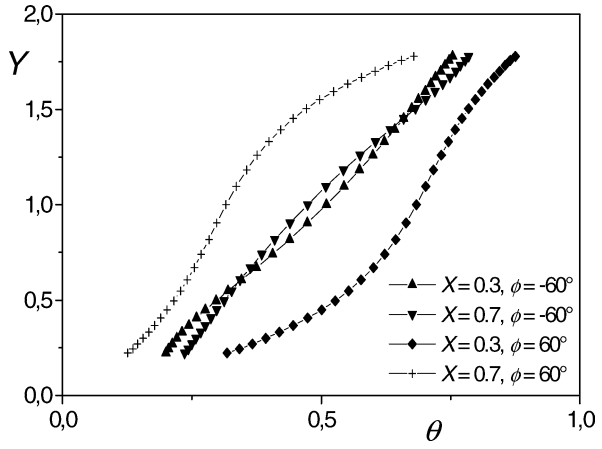

Fig. 7. Inclination angle effect on the temperatures of the vertical walls of the inner body for $R_k = 1$ and $Ra = 7.5 \times 10^4$. ($X = 0.3$: left wall and $X = 0.7$: right wall.)

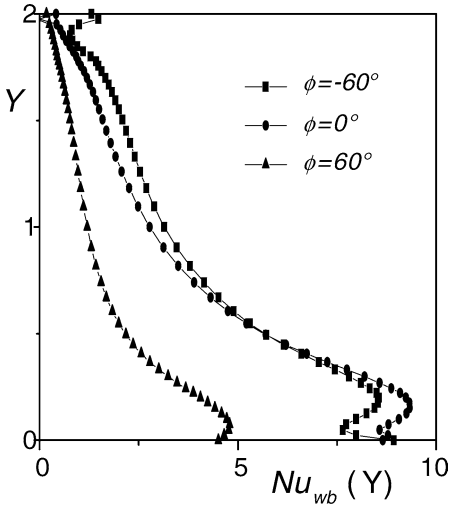

(a) *wb*

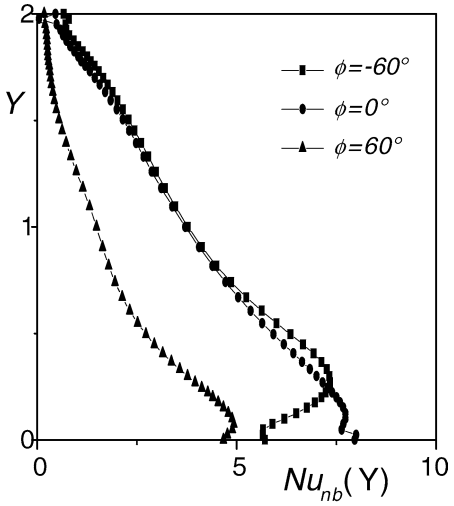

(b) *nb*

Fig. 8. Local Nusselt number on the hot wall for $R_k = 1$ and $Ra = 7.5 \times 10^4$.

by the inner body and the insulated walls, and therefore a large quantity of cold air can lick the hot wall at low ϕ. A slight difference between $Nu_{wb}(Y)$ at $\phi = 0°$ and $-60°$ is noted.

At $\phi = 60°$, the pattern of $Nu_{nb}(Y)$ (Fig. 8(b)) is quite similar to the one of $Nu_{wb}(Y)$ (Fig. 8(a)), which explains again the resemblance of the isotherms obtained for the two cavities (*wb* and *nb*) at $\phi = 60°$. $Nu_{nb}(Y)$ is largely enhanced with decreasing ϕ from 60° to 0° or −60°. This is explained one more time by the circulation that becomes stronger at low values of ϕ. $Nu_{nb}(Y)$ is almost the same for $\phi = -60°$ and $\phi = 0°$, except near the bottom hot wall where we note a slight increase of $Nu_{nb}(Y)$ obtained for $\phi = 0°$ with respect to the one corresponding to $\phi = -60°$. This is because in this region the air is warmer for $\phi = -60°$ than for $\phi = 0°$ as shown in Fig. 6(b).

Local Nusselt number structures cannot provide us with an exact idea on the effects of inclination angle ϕ and presence of inner body on total heat transfer inside the enclosure, so we judged useful the survey of the average Nusselt number.

Fig. 9 shows the average Nusselt number *Nuw* as a function of the inclination angle ϕ for a partitioned (*wb*) and an empty cavity (*nb*) for a Rayleigh number $Ra = 7.5 \times 10^4$.

The influence of the inner body is clearly seen for inclination angles ϕ greater than −30° by a pronounced decrease in the average Nusselt number with respect to the empty cavity. This decrease is nearly the same for ϕ ranged between −15° and 60°. It is also seen that both the average Nusselt numbers Nuw_{wb} and Nuw_{nb} decrease when ϕ is increased from −30° to 60°. As a matter of fact, the above discussions explain the behaviour of the average Nusselt number (shown in Fig. 9).

5.1.2. *Effect of* ΔT

Table 2 shows the average Nusselt number *Nuw* for three values of maximal difference temperature ΔT. The inclination angle and the thermal conductivity ratio were fixed at $\phi = -30°$ and $R_k = 1$, respectively. To respect the Boussinesq approximation, the maximal value of ΔT is taken equal to 30 K.

The average Nusselt number increases with increasing ΔT. In fact, the buoyancy force increases with ΔT. This causes an increase in the mass flow rate between the hot and cold parts of the cavity. Thus, the cold air coming from the cold part of the

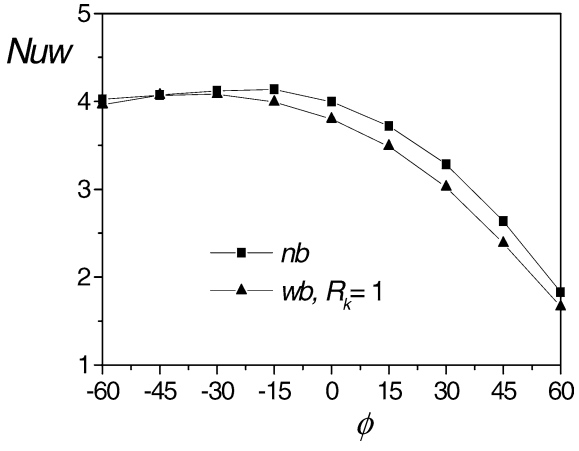

Fig. 9. Average Nusselt number *Nuw* versus the inclination angle ϕ at $Ra = 7.5 \times 10^4$.

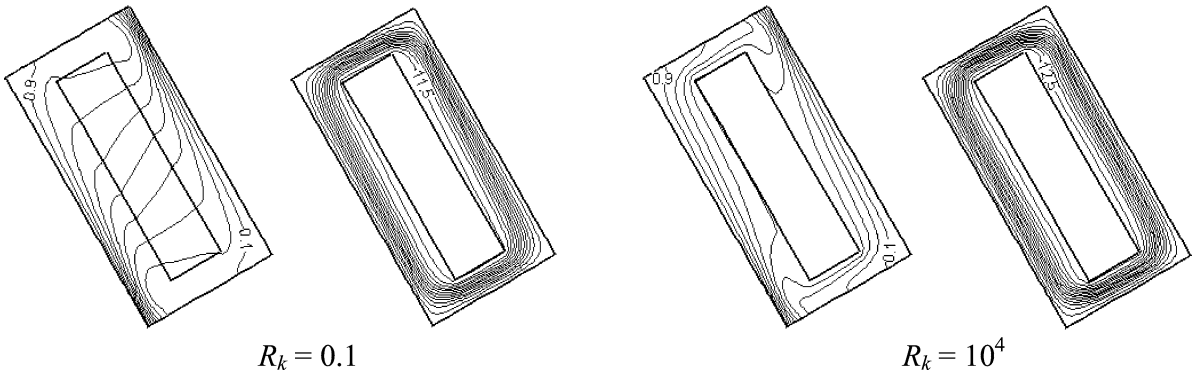

Fig. 10. Isotherms and streamlines for $Ra = 7.5 \times 10^4$, $\phi = -30°$, $\Delta\theta = 0.1$ and $\Delta\psi = 1$.

Table 2
Average Nusselt number versus ΔT for $R_k = 1$, $Pr = 0.71$ and $\phi = -30°$

ΔT [K]	Ra	Nuw_{wb}	Nuw_{nb}
5	1.25×10^4	1.99	2.63
20	5×10^4	3.56	3.73
30	7.5×10^4	4.08	4.13

cavity is pushed closer to the hot wall, so the local Nusselt number is enhanced along the hot wall. This means an increase in the average Nusselt number. Notice, however, that the increase of ΔT from 5 to 30 produces an increase in the average Nusselt numbers Nu_{wb} and Nu_{nb} by about 51% and 36%, respectively. Indeed, at high values of ΔT, the resistance of the inner body to the flow tends to become negligible than at lower values of ΔT because the boundary layers become thinner and the central core of the fluid region becomes relatively stagnant as ΔT increases.

5.1.3. Effect of R_k

Fig. 10 shows isotherms and streamlines distributions for two extreme values of R_k (0.1 and 10^4) at $Ra = 7.5 \times 10^4$ and $\phi = -30°$. We note that the thermal conductivity of the inner body affects strongly the isotherm structures. At large R_k ($R_k = 10^4$), the isotherms move out of the inner body: the inner body has a homogeneous temperature, due to its higher conductivity. This temperature is nearly equal to the average temperature T_o of the hot and cold walls. As a result, when R_k increases from 0.1 to 10^4, the temperature of the bottom part of the inner body increases while the temperature of its top part decreases. Hence, the air temperature becomes higher in the lower passage and weaker in the upper passage. Thus, the hot fluid circulating in the upper passage transfers an important portion of its sensible heat through the inner body to the cold fluid circulating in the lower passage instead of transporting it the whole path toward the cold wall of the cavity. In this way, the high thermal conductivity of the inner body reduces the overall heat transfer by natural convection between the hot and cold walls of the cavity. The streamlines obtained for $R_k = 0.1$ and 10^4 are quite similar with a slight increase in the value of the maximum stream function in the case of $R_k = 10^4$.

At $Ra = 7.5 \times 10^4$, the relation between Nuw and R_k for different inclination angles ϕ is shown in Fig. 11. As can be seen,

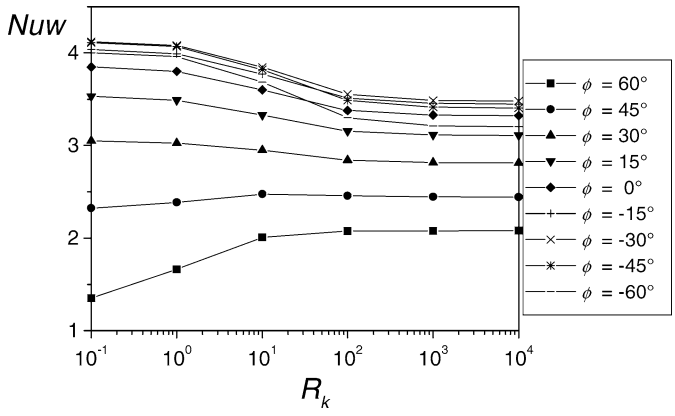

Fig. 11. Relation between R_k and average Nusselt number Nuw for $Ra = 7.5 \times 10^4$.

Nuw decreases with increasing R_k for $\phi \leqslant 30°$ and, particularly, a significant decrease can be seen at R_k ranged between 0.1 and 10^2. This implies that the suppression effect of the inner body on heat transfer becomes larger as R_k increases for $\phi \leqslant 30°$. However, for $\phi \geqslant 45°$, Nuw increases with increasing R_k, and especially for R_k ranged between 0.1 and 10 where a remarkable increase can be noted. This implies that the enhancement effect of the inner body on the heat transfer becomes important for $0.1 \leqslant R_k \leqslant 10$ and $\phi \geqslant 45°$. On the other hand, independently of the value of ϕ, Nuw is nearly constant when R_k exceeds 10^2.

5.2. Results accounting for radiation ($\varepsilon \neq 0$)

The computations were carried out for the same parameters studied in the case without radiation, in addition to the parameter ε characterising the radiation heat flux. Thus the effects of the following parameters (ε, ϕ, ΔT, R_k) are considered.

5.2.1. Effect of ε

Average hot wall Nusselt number Nuw is plotted in Fig. 12 as a function of the inner body surface emissivity ε_{ib}, with the cavity walls surface emissivity ε_w as a parameter. The numerical results are obtained for the following parameters: $\phi = 0°$, $\Delta T = 30$ K, $Nr = 21.14$ and $R_k = 1$.

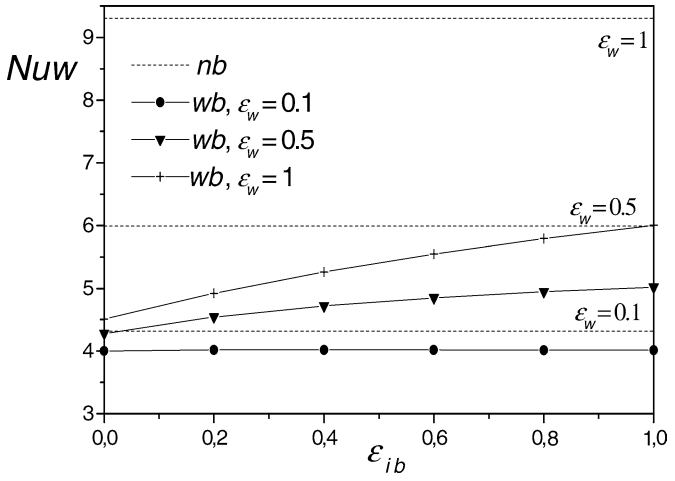

Fig. 12. Average hot wall Nusselt number as a function of the inner body emissivity ε_{ib} for $\phi = 0°$, $\Delta T = 30$ K and $R_k = 1$.

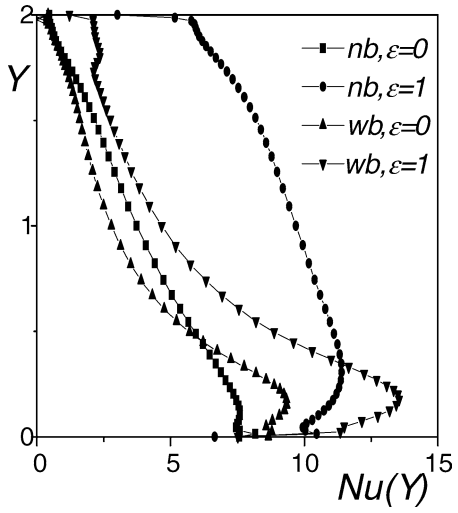

Fig. 13. Local Nusselt number on the hot wall for $\phi = 0°$, $R_k = 1$ and $Ra = 7.5 \times 10^4$.

In all cases, the average Nusselt number increases with increasing ε_w. To reduce the total heat transfer rate, surfaces with low emissivities are required for the walls of the cavity and the inner body. At lower values of the cavity walls emissivity ($\varepsilon_w = 0.1$), the average Nusselt number for a cavity with an inner body Nu_{wb} is insensitive to ε_{ib} and is slightly lower than Nu_{nb} corresponding to the same value of ε_w. As ε_w increases, Nu_{wb} becomes larger and increases with increasing ε_{ib}. The rate of increase in the value of Nu_{wb} with ε_{ib} is more important as ε_w approaches its maximum value ($\varepsilon_w = 1$).

From the curves pattern, it is clearly shown that the emissivity ε_w affects considerably the average Nusselt number. Furthermore, the average Nusselt number Nu_{nb} at $\varepsilon_w = 0.5$ is equal to the higher value that can be achieved by Nu_{wb} (i.e. at $(\varepsilon_{ib}, \varepsilon_w) = (1, 1)$). Thus, since the effect of ε_w on Nu_{nb} is more important than that on Nu_{wb}, this yields to a rapid increase in the value of Nu_{nb} with ε_w if compared with the response of Nu_{wb} to the increase of ε_w. This can be attributed to the fact that the inner body acts as an obstacle with regard to the radiative heat coming from the hot wall.

In the following paragraphs, ε_{ib} and ε_w are equal and are simply noted ε.

Fig. 13 shows the variation of the local Nusselt number $Nu(Y)$ along the hot wall in presence and in absence of the thermal radiation for a partitioned and an empty cavity. In fact, Fig. 13 brings an explanation to the variation of the average Nusselt number *Nuw*, presented in Fig. 12. It is clearly shown in Fig. 13, that the thermal radiation produces a large increase of $Nu(Y)$; particularly in the empty cavity. Notice, however, that the inner body reduces considerably $Nu(Y)$ because it obstructs the radiative heat flux emitted by the hot cavity wall. Consequently, the net radiative heat flux at the hot wall, Q_r (which is counted in *Nuw*) is lower in the case of a partitioned cavity than in the case of an empty one.

5.2.2. *Effect of* ϕ

Isotherms and streamlines patterns in both cases *wb* and *nb*, for three inclination angles ϕ of 60, 0 and −60 degrees are plotted in Fig. 14. The same parameters are used as in the pure natural convection case (Fig. 6) in an attempt to show the effect of the thermal radiation heat flux on the isotherms and streamlines. The inclinations of isotherms near the insulated walls and near the inner body boundaries are due to the importance of the radiative heat fluxes exchanged between the radiative surfaces. From the temperature contours, it appears that the radiation heat transfer produces a good standardization of temperature in each part of the cavity. This is attributed to the fact that the radiation heat transfer reduces the temperature difference between the radiative surfaces located in each part of the cavity as shown in Fig. 15 for the vertical surfaces of the inner body and the isothermal walls. Indeed, the temperature of the vertical left surface of the inner body increases under the radiation effects of the hot wall; whereas the temperature of the vertical right surface of the inner body decreases because it emits radiation toward the cold wall. Thus a channel is generated between the hot wall and the inner body and another is generated between the cold wall and the inner body.

Concerning the streamlines, as the case of pure natural convection (see Fig. 6) and for two kinds of cavities (*wb* and *nb*), the increase of the inclination angle ϕ reduces largely the velocity of the flow in the cavity as shown in the streamline structures, especially for positive values of ϕ. On the other hand, the radiation heat transfer increases the air circulation in the cavity. This is due to the increase in difference between the average air temperatures in the left and right part of cavity under the radiation effect.

The effects of inclination angle on local Nusselt number distribution on the hot wall $Nu(Y)$, for partitioned and empty cavities are presented in Fig. 16. As in the pure natural convection case (Fig. 8), the local Nusselt number $Nu(Y)$ obtained for $\phi = 60°$ is lower than those corresponding to $\phi = 0°$ or $-60°$. We also note that the radiation exchange increase considerably $Nu(Y)$ for all values of ϕ. This increase is more pronounced in the case of the empty cavity than in the case of the partitioned one owing to the shadow effect to the radiation produced by the inner body in the last case. Therefore, as shown in Fig. 17, the

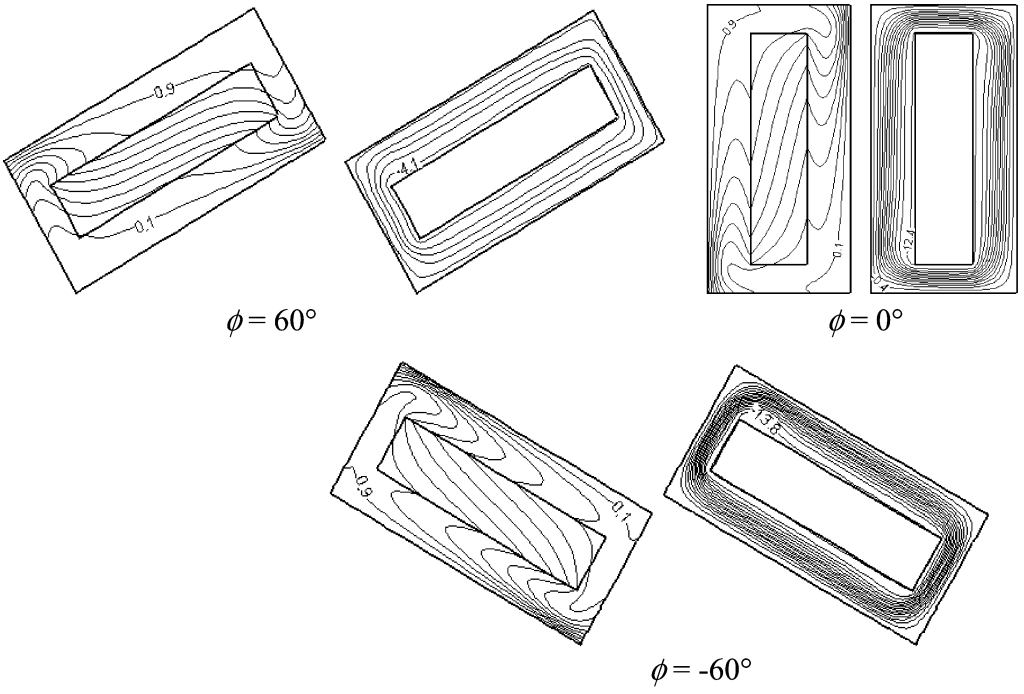

(a) *wb*

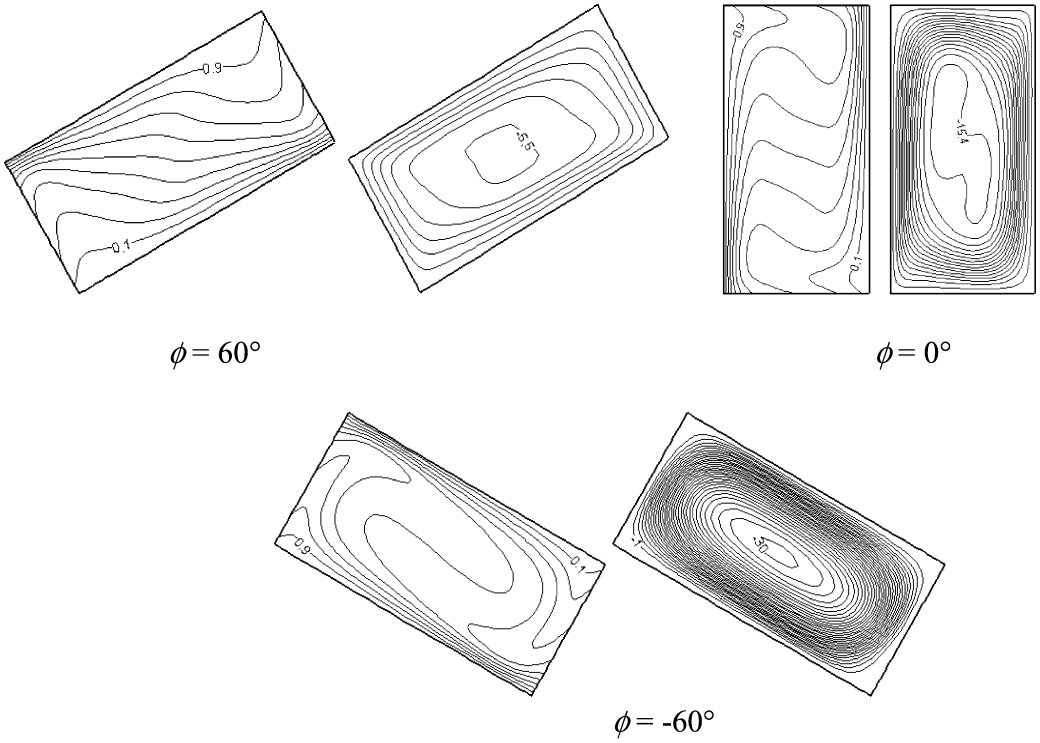

(b) *nb*

Fig. 14. Isotherms and streamlines for $R_k = 1$, $Ra = 7.5 \times 10^4$, $Nr = 21.14$, $\varepsilon = 1$, $\Delta\theta = 0.1$ and $\Delta\psi = 1$.

variation of average Nusselt number *Nuw* according to ϕ is the same as in pure natural convection, but the radiation heat transfer produces an important increase of *Nuw*, particularly in the case of the empty cavity.

5.2.3. Effect of ΔT

The effect of temperature difference ΔT is investigated for $\phi = -30°$, $R_k = 1$ and $\varepsilon = 1$.

Three values of ΔT (5 K, 20 K, and 30 K) as in the pure

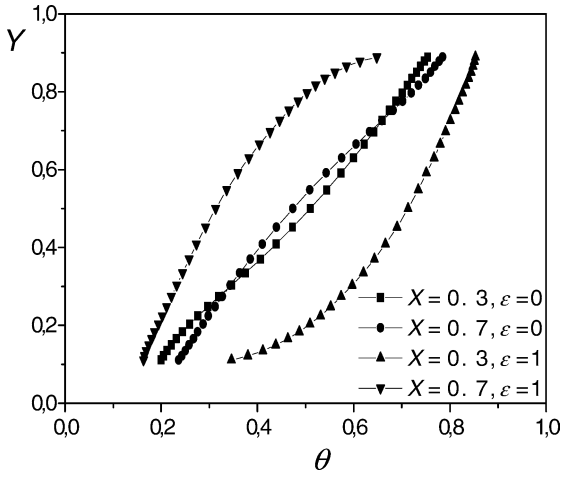

Fig. 15. Radiation effect on walls temperature distribution at $\phi = -60°$, $R_k = 1$ and $Ra = 7.5 \times 10^4$.

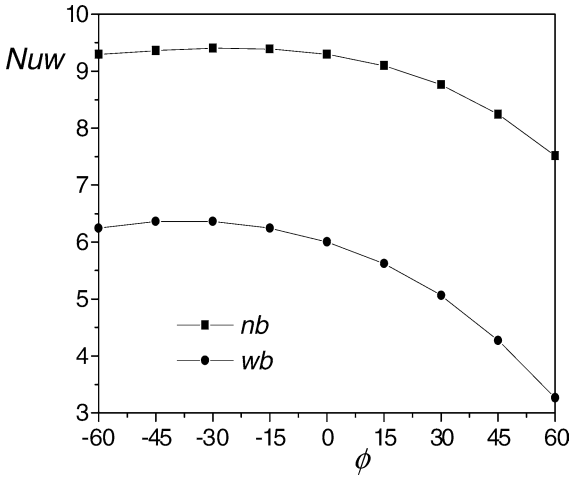

Fig. 17. Average hot wall Nusselt number *Nuw* as a function of the inclination angle ϕ for $Ra = 7.5 \times 10^4$, $Nr = 21.14$ and $\varepsilon = 1$.

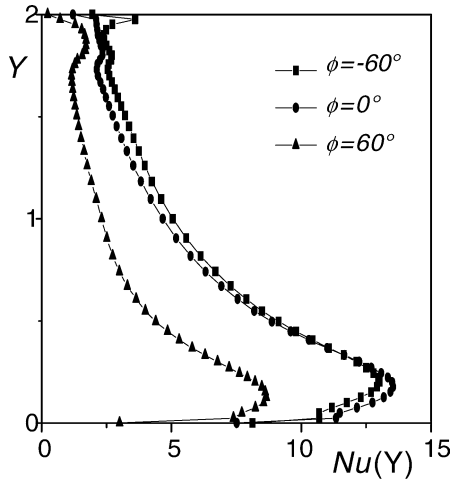

(a) *wb*

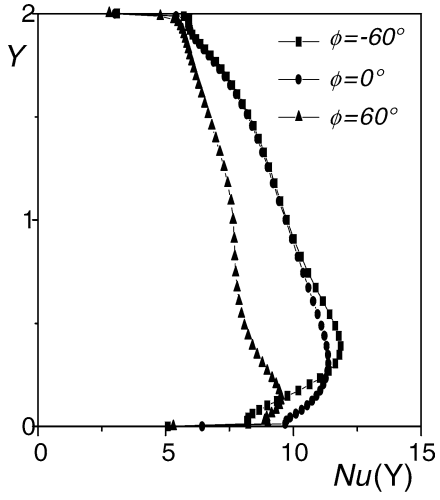

(b) *nb*

Fig. 16. Local Nusselt number on the hot wall for $R_k = 1$, $Ra = 7.5 \times 10^4$, $Nr = 21.14$ and $\varepsilon = 1$.

Table 3
Average hot wall Nusselt numbers versus ΔT for $R_k = 1$, $\phi = -30°$ and $\varepsilon = 1$

ΔT [K]	*Ra*	Nu_{wb}	Nu_{nb}
5	1.25×10^4	3.45	8.04
20	5×10^4	5.68	9.08
30	7.5×10^4	6.36	9.40

natural convection case are chosen to show the effect of the radiation heat transfer on *Nuw*. Table 3 shows that for both cases (*nb* and *wb*), *Nuw* increases with increasing ΔT and under the radiation heat transfer effect. In fact, the increase of ΔT causes an increase in both the buoyancy force and the radiation number *Nr*, which produce in their turn an increase in the convective and radiative contributions in *Nuw*, respectively. The shadow effect caused by the inner body to the thermal radiation explains one more time the fact that Nu_{nb} is greater than Nu_{wb}.

5.2.4. *Effect of* R_k

Fig. 18 presents the isotherms and streamlines for $\Delta T = 30$ K ($Ra = 7.5 \times 10^4$), $\phi = -30°$, $\varepsilon = 1$ and two values of R_k (0.1 and 10^4). As in pure natural convection case ($\varepsilon = 0$), at large R_k ($R_k = 10^4$) the inner body has a homogeneous temperature, which approaches the average temperature T_o. Thus, at $R_k = 10^4$ the radiative surfaces temperatures of the inner body are nearly equal to T_o; which explains that the radiation effect is negligible on the isotherms and streamlines near the inner body. Notice, however, that the influence of the radiation exchange on the isotherms near the horizontal walls of the cavity is very obvious. For $R_k = 0.1$, two channels are generated under the radiation effect, and the air flow is accelerated in comparison to the case of $\varepsilon = 0$. For both values of R_k, the streamline patterns are quite similar to those obtained for $\varepsilon = 0$.

The average Nusselt number *Nuw* as a function of the thermal conductivity ratio R_k for $Ra = 7.5 \times 10^4$ and various inclination angles ϕ is presented in Fig. 19. The behaviour of the curves presented in Fig. 19 is different from that seen in pure natural convection case. This is valid for all values of ϕ, except for $\phi \geqslant 45°$ (see Fig. 11). Indeed, for all values of ϕ, *Nuw* is

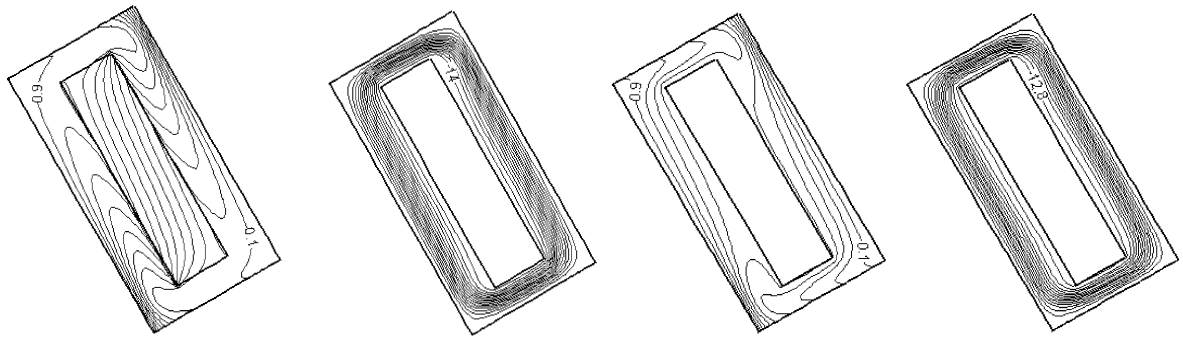

Fig. 18. Isotherms and streamlines for $Ra = 7.5 \times 10^4$, $\phi = -30°$, $Nr = 21.14$, $\varepsilon = 1$, $\Delta\theta = 0.1$ and $\Delta\psi = 1$.

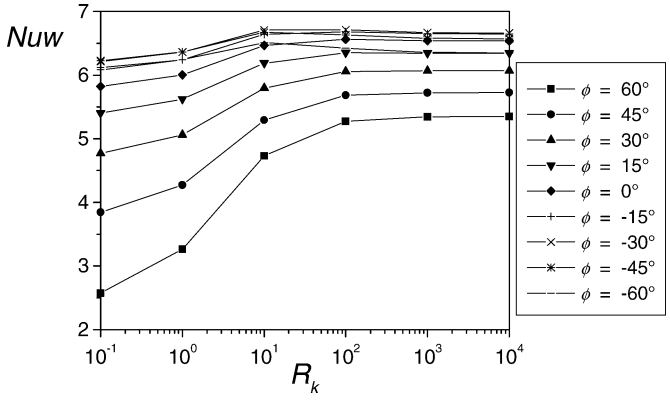

Fig. 19. Relation between R_k and average Nusselt number *Nuw* for $Ra = 7.5 \times 10^4$, $Nr = 21.14$ and $\varepsilon = 1$.

largely enhanced by an increase of R_k from 10^{-1} to 10^2. For R_k superior to 10^2, the variation of *Nuw* against R_k is negligible. Furthermore, the response of *Nuw* to the variation of R_k is important as ϕ increases.

On the other hand, a comparison between Fig. 19 and Fig. 11 shows that the radiation exchange produces a net increase in the average Nusselt number *Nuw* for all values of ϕ and R_k. This increase is especially important at high value of R_k. In fact, when R_k is high, the temperature of the inner body is uniform and equal nearly to the average temperature T_o. Thus, the net radiative flux along the hot wall and consequently *Nuw* are high. However, when R_k is weak, the temperature of the vertical left surface of the inner body is greater than T_o, so the net radiative flux along the hot wall is less important than for a high value of R_k.

6. Conclusion

The combined radiation-natural convection heat transfer in an inclined partitioned enclosure has been investigated numerically. Both cases: enclosure with or without inner body, have been considered. The investigation shows results of the effects of inclination angle ϕ, thermal conductivity ratio R_k, maximal difference temperature ΔT in the presence and in the absence of radiation heat transfer. The effect of the emissivities of radiative surfaces was also investigated.

This study has shown the response of heat transfer, isotherms and streamlines structures to the variations in the above mentioned parameters (ϕ, ΔT, R_k), firstly in pure natural convection, and secondly when the radiative heat transfer is taken into account.

Three principal conclusions can be drawn:

(1) For both cavities (*wb* and *nb*), and either in the pure natural convection ($\varepsilon = 0$) or in the combined mode ($\varepsilon \neq 0$), *the inclination angle* ϕ affects strongly the isotherm structures and the streamline values in the cavity. Concerning the average Nusselt number, the effect of ϕ is important only for its positive values. Indeed, *Nuw* decreases with increasing ϕ for $\phi > 0°$, however, there is a little change in *Nuw* against the negative ϕ values.

(2) *Thermal conductivity ratio* R_k affects the isotherm distribution in inner body, thus it affects also isotherms in the entire cavity. The effect of thermal conductivity ratio R_k on the average Nusselt number *Nuw* depends upon the value of the inclination angle ϕ. In the presence of the radiation heat transfer and independently of ϕ, *Nuw* increases with increasing R_k. However, in the absence of the radiation heat transfer ($\varepsilon = 0$) and when R_k is varied from 0.1 to 10^2, *Nuw* increases for $\phi \geqslant 45°$ and decreases for $\phi \leqslant 30°$. When R_k exceeds 10^2, its effect on *Nuw* is negligible.

(3) *Radiation heat transfer* increases considerably the average Nusselt number, particularly in the absence of the inner body. It also standardizes temperatures of radiative surfaces in each part of the cavity, thus the structures of isotherms are completely different from those obtained in pure natural convection.

References

[1] T. Nishimura, M. Shirashi, F. Nagasawa, Y. Kawamura, Natural convection heat transfer in enclosures with multiple vertical partitions, Int. J. Heat Mass Transfer 31 (8) (1988) 1679–1686.

[2] W.-S. Fu, J.-C. Perng, W.-J. Shieh, Transient laminar natural convection in an enclosure partitioned by an adiabatic baffle, Numer. Heat Transfer A 16 (1989) 325–350.

[3] J.M. House, C. Beckermann, T.F. Smith, Effect of a centred conducting body on natural convection heat transfer in an enclosure, Numer. Heat Transfer A 18 (1990) 213–225.

[4] M. Ciofalo, T.G. Karayiannis, Natural convection heat transfer in a partially or completely-partitioned vertical rectangular enclosure, Int. J. Heat Mass Transfer 31 (1) (1991) 167–179.
[5] J.Y. Oh, M.Y. Ha, K.C. Kim, Numerical study of heat transfer and flow of natural convection in an enclosure with a heat-generating conducting body, Numer. Heat Transfer A 31 (1997) 289–304.
[6] M.Y. Ha, M.J. Jung, Y.S. Kim, A numerical study on transient heat transfer and fluid flow of natural convection in an enclosure with a heat-generating conducting body, Numer. Heat Transfer A 35 (1999) 415–434.
[7] M.Y. Ha, M.J. Jung, A numerical study on three-dimensional conjugate heat transfer of natural convection and conduction in a differentially heated cubic enclosure with a heat-generating cubic conducting body, Int. J. Heat Mass Transfer 43 (2000) 4229–4248.
[8] E. Ramos, A. Castrejon, M. Gordon, Natural convection in a two-dimensional square loop, Int. J. Heat Mass Transfer 33 (5) (1990) 917–930.
[9] T. Kimura, M. Takeuchi, T. Miyanaga, Natural-convection heat transfer in inclined rectangular enclosure, Trans. JSME B 58 (547) (1992) 850–856.
[10] D.W. Larson, R. Viskanta, Transient combined laminar free convection and radiation in a rectangular enclosure, J. Fluid Mech. 78 (1976) 65–85.
[11] G. Lauriat, Combined radiation–convection in gray fluids enclosed in vertical cavities, J. Heat Transfer 104 (1982) 609–615.
[12] G. Lauriat, Numerical study of the interaction of natural convection with radiation in nongray gases in a narrow vertical cavity, Int. J. Heat Mass Transfer (1982) 153–158.
[13] A. Yücel, S. Acharya, M.L. Williams, Natural convection and radiation in a square enclosure, Numer. Heat Transfer A 15 (1989) 261–278.
[14] A. Draoui, F. Allard, C. Beghein, Numerical analysis of heat transfer by natural convection and radiation in participating fluids enclosed in square cavities, Numer. Heat Transfer A 20 (1991) 253–261.
[15] C. Balaji, S.P. Venkateshan, Interaction of surface radiation with free convection in a square cavity, Int. J. Heat Fluid Flow 14 (3) (1993) 260–267.
[16] M. Kassemi, M.H.N. Naraghi, Analysis of radiation natural convection interactions in 1-g and low-g environments using the discrete exchange factor method, Int. J. Heat Mass Transfer 36 (12) (1993) 4141–4149.
[17] C. Balaji, S.P. Venkateshan, Correlations for free convection and surface radiation in a square cavity, Int. J. Heat Fluid Flow 15 (3) (1994) 249–251.
[18] S.K. Mahapatra, S. Sen, A. Sarkar, Interaction of surface radiation and variable property natural convection in a differentially heated square cavity—a finite element analysis, Int. J. Numer. Methods Heat Fluid Flow 9 (4) (1999) 423–443.
[19] G. Colomer, M. Costa, R. Cònsul, A. Oliva, Three-dimensional numerical simulation of convection and radiation in a differentially heated cavity using the discrete ordinates method, Int. J. Heat Mass Transfer 47 (2004) 257–269.
[20] L.C. Chang, K.T. Yang, J.R. Lloyd, Radiation-natural convection interactions in two dimensional complex enclosures, J. Heat Transfer 105 (1983) 89–95.
[21] H. Nakamura, Y. Asako, Combined free convection and radiation heat transfer in rectangular cavities with a partition wall, Trans. JSME B 50 (459) (1984) 2647–2654.
[22] A. Mezrhab, L. Bchir, Radiation-natural convection interactions in partitioned cavities, Int. J. Numer. Methods Heat Fluid Flow 9 (2) (1999) 186–203.
[23] C.Y. Han, S.W. Baek, The effects of radiation on natural convection in a rectangular enclosure divided by two partitions, Numer. Heat Transfer A 37 (2000) 249–270.
[24] A. Mezrhab, H. Bouali, C. Abid, Radiation-natural convection interactions in an enclosure with a heat-generating conducting body, in: Congrès Français de Thermique SFT, 25–28 mai 2004, Presqu'île de Giens, France.
[25] A. Mezrhab, H. Bouali, C. Abid, Modelling of combined radiative and convective heat transfer in an enclosure with a heat-generating conducting body, Int. J. Comput. Methods 2 (3) (2005) 431–450.
[26] S.V. Patankar, Numerical Heat Transfer and Fluid Flow, Hemisphere/McGraw-Hill, Washington, DC, 1980.
[27] A. Mezrhab, M. Bouzidi, Computation of view factors for surfaces of complex shape including screening effects and using a boundary element, Engrg. Comput.: Int. J. Comput. Aided Engrg. Software 22 (2) (2005) 132–148.